Quantitative MRI Measurements of Function, Perfusion and Viability in

Microembolized, Moderately Ischemic Myocardium

by

Loi Do

THESIS

Submitted in partial satisfaction of the requirements for the degree of

MASTER OF SCIENCE

In

Biomedical Imaging

in the

Acknowledgement

Quantitative MRI Measurements of Function, Perfusion and Viability in Microembolized,
Moderately Ischemic Myocardium
Loi Do

Abstract

 Introduction: Multiple factors make assessment of microembolization clinically challenging.
We aimed to 1) provide detailed analysis and comparison of infarct healing in ischemic
myocardium with and without microemboli and 2) validate MRI measurements against
histochemical/histological staining.

Methods: Animals either served as controls (group I, n=8) or were subjected to one of two
percutaneous coronary interventions (PCI) (n=8/group): 1) 45 min occlusion of the left anterior
descending (LAD) coronary artery followed by reperfusion (group II) and 2) the same duration
of occlusion followed by microemboli delivery prior to reperfusion (group III). Cine, perfusion
and delayed contrast enhanced MRI (DE-MRI) were performed on a 1.5T scanner after 3 days
and 5 weeks. The left ventricles (LV) were sliced and stained with TTC (triphenyltetrazolium
chloride) and Masson trichrome to visualize, delineate and compute scar tissue planemetrically
in groups II and III, respectively.

Results: Both intervention groups showed on MRI an increase in end systolic volume and
decrease in ejection fraction compared to controls and these changes were more pronounced in
group III than II. Unlike group II, group III showed persistent perfusion deficits. Small but
homogeneous MI on DE-MRI was visible in group II (1.3±0.9g) with substantially larger MI in
group III (7.7±0.5g), however, the resorption was significantly smaller in group III (22%) than
group II (60%, $P<0.05$). Postmortem TTC revealed similar extent of scar tissue to DE-MRI in
groups II (1.6±1.0g) and III (group III 9.2±1.6g) at 5 weeks. Histology revealed larger infarct
extent in group II (2.8±0.4g, $P<0.05$) and III (10.5±1.5, $P<0.01$) than DE-MRI.

Conclusion: MRI detected structural and functional changes in moderately ischemic

myocardium with and without microemboli. In ischemic microembolized myocardium, homogeneous infarct, patchy microinfarct and compensatory hypertrophy were visible at 5 weeks. Microvascular obstruction exacerbates the development of compensatory hypertrophy. DE-MRI has the potential to monitor infarct resorption after PCI, but has limited spatial resolution for estimating true infarct extent, which should be taken into account when used to testing the efficacy of newer cardioprotective therapies and distal protective devices in improving LV function.

TABLE OF CONTENTS

LIST OF FIGURES

LIST OF TABLES

Introduction

Ischemic myocardium is a major cause of morbidity and mortality worldwide. Percutaneous coronary intervention (PCI) performed in severely stenosed ischemic myocardium or occluded coronary artery with acute myocardial infarction (AMI), which is the most common intervention for revascularization. Early diagnosis of structural and functional changes in ischemic myocardium after PCI is critical for initiation of effective treatment strategies and improved prognosis in patients.

Large variation in volume/size of microemboli during PCI, myocardial infarct (MI) size, imaging time after revascularization and lack of biopsy, makes it challenging to study microemboli effects clinically. The effects of microemboli on left ventricular (LV) function, perfusion and viability have been recently recognized by major interventional and cardiology societies (1-7). Clinical trials have suggested that the speed of infarct repair depends on multiple factors, including: infarct mass, perfusion, microvascular obstruction (MVO) and hemorrhage (8-10). Clinical studies showed that MVO portends a poor prognosis (11). MVO in AMI it delays infarct healing and accentuates myocardial hypertrophy (12). The focus has shifted to the clinical importance of coronary microemboli and microinfarcts. Our lab has established state-of-the-art imaging protocols for measuring LV function, perfusion and viability after coronary microembolization in swine model (13-17). This project is designed to provide simulation of microinfarct as it occurs in routine coronary revascularization in severe coronary stenosis. It also demonstrates the potential of MRI in detecting the effects of microemboli on ischemic myocardium compared with solely ischemic myocardium and controls using LV function, perfusion and viability indices.

Materials and Methods

Experimental animals received humane care in compliance with the Guide for the Care and Use of Experimental Animals formulated by the University of California San Francisco Institutional Animal Care and Use Committee (IACUC). The pig heart in situ with regional myocardial ischemia and reperfusion is of unique translational value (18). Cardiac size, heart rate and blood pressure are similar to those in humans as well as the temporal and spatial development of myocardial infarct. Conceptually, all cardioprotective phenomena, including hibernation, ischemic preconditioning, ischemic postconditioning, and remote conditioning, have been demonstrated in pig hearts. Pigs can be repeatedly anesthetized, subjected to precise microemboli load and infarct time, invasively and non-invasively monitored in ways that humans cannot.

Experimental models

Animals either served as controls (n=8, Group I) or were subjected to interventions (n=8 per group). Animals subjected to interventions were randomly assigned to groups as follows: Group II animals were subjected to 45 min angioplasty balloon (Cook, Chicago, Ill) occlusion of the left anterior descending (LAD) coronary artery followed by reperfusion and Group III animals were subject to the same intervention followed by microemboli ($32mm^3$ volume, 120K count, 40-120μm diameter/1ml saline) delivery prior to reperfusion to avoid back flow (Figure 1)(2-4, 14, 15, 17, 19).

The control group was designed to assess the LV function and histology, therefore they were imaged using the same cine MR imaging sequence as the interventional groups at 3 days and 5 weeks followed by euthanasia and all postmortem procedures were identical to the interventional groups. The interventional groups simulate clinical models of brief ischemic injury where: 1) microemboli resulting from erosion or rupture of atherosclerotic plaque are dislodged during

2

navigation of guidewires, endovascular catheters, distal filtration devices and during deployment of stents or inflation of a balloon across the lesion; 2) PCI performed with clinically available distal filtration devices with pore sizes >120μm allow the passage of microemboli <120μm (20-31). The volume/sizes of microemboli, duration of LAD occlusion/reperfusion and imaging time after intervention were defined and held constant. The volume/sizes of delivered microemboli were based on an autopsy studies in patients (21, 32, 33). Farm pigs (n=16, 30-32 kg at 3 days and 49-53kg at 5 weeks) were premedicated using acepromazine (0.5 mg/kg body weight, Boehringer Ingelheim Vet Medica Inc, St Joseph, MO, USA) and ketamine (20 mg/kg body weight, Fort Dodge Animal Health, Fort Dodge, IA, USA). Isoflurane/oxygen inhalation (2-5%/2-3 L/min) (Henry Schein Animal Health, Dublin, OH, USA) was given through an endotracheal tube during the intervention and imaging. Prior to coronary intervention, a vascular sheath was percutaneously placed in the femoral artery. The animals received heparin (100 IU/kg body weight, Fresenius Kabi, Schaumburg IL USA), lidocaine (10 mg/kg body weight, Hospira Inc, Lake Forrest, IL, USA) and saline manually (10 ml/kg/hr, Baxter Healthcare, Deerfield, IL, USA) via an ear vein. ECG, heart rate, blood pressures, O2-sat, PCO2 and body temperature were monitored continuously during the interventions and imaging.
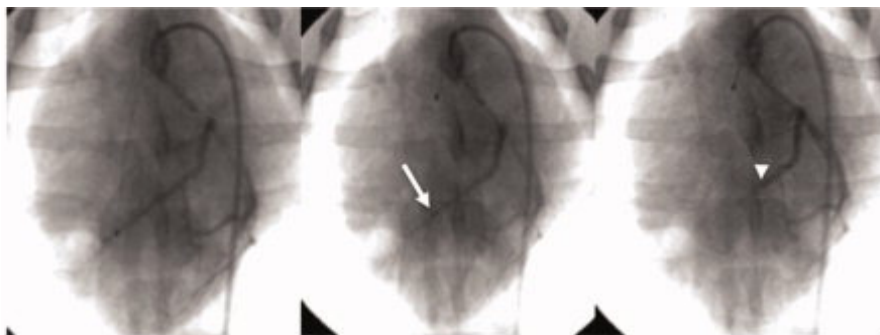
Figure 1. X-ray fluoroscopy of a representative Group III animal before (left), during (middle) and after (right) 45 min occlusion of the LAD coronary artery. The site of balloon occlusion (white arrow) and the beginning of delayed filling of iodinated contrast media (arrowhead) confirm delivery of microemboli.

imaging. The LAD was selected as prior studies found that 89% of microemboli (120-250 μm) are lodged in the LAD (20, 21). The second diagonal branch of LAD was used as an anatomical

3

landmark for LAD occlusion and microemboli delivery because LAD coronary occlusion at proximal levels increases the risk of refractory ventricular fibrillation and death (34). All surgical procedures, blood sampling and imaging were performed while the animals were under anesthesia. Blood samples (5ml) were obtained from all animals at baseline, 24hrs and 72hrs for measuring cardiac injury biomarkers (creatine-kinase and troponin I) using radioimmunoassay. Cardiac injury biomarkers (creatine-kinase and troponin I) were used to confirm the presence of myocardial infarcts (MI). Animals subjected to interventions received trimethoprim/sulfamethoxazole (15mg/kg body weight orally twice daily for 5 days) and carprofen (4mg/kg body weight orally daily for 3 days) after intervention.

MRI

MRI was performed using a 12-channel coil on a 1.5T MR system (GE Medical Systems, WI). To assess cardiac function and LV dimension, a stack of continuous short-axis slices covering the whole LV were acquired with ECG-gated steady-state free-precession (SSFP) cine-images during repeated breath holds. Cine MRI parameters were: repetition time (TR)/echo time (TE)/flip angle=3.5ms/1.8ms/70°, slice thickness=6mm without gap, field of view (FOV)=26×26cm; matrix size=160x152; number of excitations (NEX)=1 and cardiac phases=16 (35). Cine MRI elucidated the changes in LV ejection fraction, end diastolic and systolic volumes, LV mass and systolic wall thickening and thickness. Global and regional quantitation of contractility in the LAD territory was necessary for defining the deleterious effects on not only the infarcted region but also the adjacent territories, which may be stunned.

Myocardial perfusion was determined in the territory distal to the site of occlusion (0.5cm above the apical tip of the heart and covered 2.5mm) using scout images for guidance. Saturation-recovery gradient echo sequence was used to track the first passage of Gd-DTPA over

4

59s (18s breath hold). . The images were acquired at 5 seconds before, during and after the administration of Gd-DTPA (0.1 mmol/kg) for a total time of 50 seconds. The imaging parameters in short axis view were: TR/TE/flip angle=4.5ms/2.2ms/20°, slice thickness=6mm without gap, FOV=26X26cm, matrix size=128x128 and acquisition time=2R-R interval (35). First pass MRI perfusion was performed in groups II and III (36). Myocardial perfusion indices that were measured included max upslope, max signal intensity and time to max signal intensity. These quantitative indices are important for understanding the functional changes of the vasculature within the LAD territory.

Inversion recovery gradient echo MRI was used for viability imaging. The images were acquired at 10min after the administration of additional dose of Gd-DTPA (0.05 mmol/kg). The imaging parameters in short (entire heart) and long (3 slices) axis views were: TR/TE/flip angle=5ms/2ms/15°; FOV=26×26cm; slice thickness=6mm without gap; read and phase matrix size=256x162, NEX=2 and inversion time (TI)=230-240ms (35). Viability MRI was performed in groups II and III. Because group I animals were not exposed to any intervention and based on regional and global function MRI findings, no first pass perfusion or DE-MRI were performed in that group of animals.

Image analysis

MR images were acquired in standardized orientations. For analyzing regional systolic wall thickening, volumes and mass were obtained on cine MRI acquired in the short axis view. The endocardial and epicardial contours were manually drawn in end systolic and end diastolic phases using *Segment* (version 1.6; URL: http://segment.heiberg.se/) (37). Regional diastolic wall thickness and systolic wall thickening was quantified in 3 slices (18, 22 and 28mm from the apex) distal to LAD occlusion and one slice at 18mm from the base (35). Each slice was divided

into 8 circumferential segments/slice. LV mass was calculated as total myocardial volume multiplied by the specific density of the myocardium (1.05g/ml). The kinetics (wash-in and wash-out) of MR contrast media were monitored over 18s during first pass of a bolus that covered 25mm (slice thickness=0.625mm) distal to the site of LAD occlusion. Changes in regional attenuation/signal intensity were measured by drawing free-hand ROIs of approximately 6-10 pixels in LV chamber blood, infarct core, peri-infarct zone and remote myocardium. Data on regional perfusion were averaged from 3 slices (18, 22 and 28mm from the apex) (35). Reproducible locations at 3 days and 5 weeks were achieved by using anatomical landmarks such as papillary muscles. The changes in regional signal attenuation/signal intensity were constructed as a function of time (peak attenuation/signal intensity). For quantification of myocardial infarct a semi-automatic threshold technique (3SD) was used after delineating endocardial and epicardial contours (35). MVO zone (hypoenhanced region) was delineated manually, measured and the extent added to myocardial infarct mass. The peri-infarct zone has been previously defined as 5±4mm from hyperenhanced infarct in humans (38) and swine (35), in which and this distance was used as a reference for our analysis.

The animals were serially (3 days and 5 weeks) monitored to correlate the effects of the interventions (16, 39-43) using non-imaging methods, such as histochemical and histological analysis, (17, 39, 44, 45) and various MRI sequences. The effects of intracoronary delivered microspheres (referred to as delivered microemboli) were determined in the presence of moderately ischemic myocardium. During scanning, breath holds for 18-24s were performed by turning off the respirator at end-expiration (46). This was accompanied with ECG gating to compensate for motion. At least one minute was given for breathing between image acquisitions.

Arterial oxygen saturation (MR compatible Oxymeter, Nonin Sensor 7500FO), heart rate and ECG (4 leads 4 electrocardiogram) showed no substantial changes during image acquisition.

Postmortem analysis

At the conclusion of the final imaging session at 5 weeks, the animals were euthanized with saturated KCl, the hearts were excised, LV isolated, weighed and sliced (~6mm thickness rings) in short axis orientation. Each ring was then incubated in 2% triphenyltetrazolium chloride (TTC) histochemical stain at 37°C for 30min to define MI. Digital images of TTC stained short-axis slices were acquired and quantified using *ImageJ* (3). Tissues were fixed using 10% formalin prior to sectioning and histologic staining. Histologic data were compared with MRI and obtained and stained with Masson trichrome (scar sizing and vascular remodeling), respectively. Histologic findings may highlight possible mechanisms of LV dysfunction.

LV function, perfusion, mass and MI were measured on MRI, histochemical (TTC) and histological stains. MR imaging was performed in groups II (n=8) and III (n=8) at 3 days and 5 weeks. At 5 weeks, TTC and hematoxilin/eosin and Masson trichrome stains were used.

Myocardial infarct on MRI/histochemical staining/histological staining was presented in grams. To characterize microembolized infarct all sections were examined under light microscopy (40-200X) and photographed using *NIS Elements-F* (Nikon, Melville, NY, USA). Microscopic photographs of all segments in the entire LV rings (7-8 slices) was measured were assembled and analyzed using planemetry to measure infarct and microinfarct sizes from 15X magnification.

Statistical analysis

Myocardial LV dysfunction, perfusion and viability on MRI, histochemical and histological stains were all analyzed using the following parameters: LV volumes, ejection

fraction, systolic wall thickening, perfusion (max upslope, time to peak and signal intensity), extent of infarct size, MVO and LV mass. Statistical analyses were performed using *GraphPad* (San Diego, CA) and the differences between 3 days and 5 weeks were determined with ANOVA. For post-hoc analysis, paired/unpaired Student's t-tests were used for intra and inter group comparisons. The Kruskal-Wallis test was used as a non-parametric test to compare independent samples (MI on MRI, histochemical and histological staining) in groups II and III at 3 days and at 5 weeks in group III. Statistical tests were considered significant when $P<0.05$. For agreements and relationships between MRI, TTC and histology measurements, Bland-Altman analysis and correlation coefficients were used, respectively. Data were presented as means ± SEM.

Results

Both intervention groups showed significant changes in LV function on cine MRI compared to controls. There were no significant differences in heart rate or blood pressure between the 3 day and 5 week studies. Physiologic parameters, such as stroke volume and O_2 saturation were not significantly different between the 3 groups over the course of 5 weeks (data not shown).
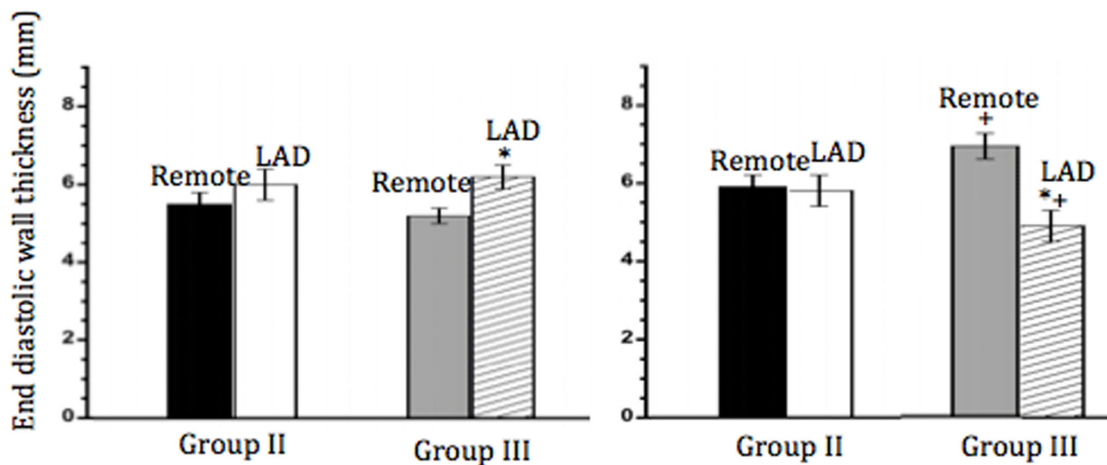

Figure 2. End diastolic wall thickness at 3 days (left bars) and 5 weeks (right bars) show very little change from 3 days to 5 weeks in regional wall thickness in group II animals whereas, wall thinning in the LAD coronary artery territory (white and striped bars) and compensatory hypertrophy in remote myocardium (black and grey bars) was evident in group III animals. * $P<0.05$ compared with remote myocardium, +$P<0.05$ compared with group II.

At the regional level, end diastolic wall thickness of the average of 3 apical slices for group II were not significantly different between 3 days and 5 weeks between the LAD territory and remote myocardium. However, in group III there was significant wall thinning in the LAD territory and compensatory hypertrophy in the remote myocardium (Figure 2). Regional systolic wall thickening revealed that the core of the infarct of group III animals was more dysfunctional than group II animals at 3 days and 5 weeks (Figure 3).

Globally, LV ejection fraction at 3 days (44.8±2.3%) was not significantly different from 5 weeks (47.1±2.2% *P*=ns), in group II animals. While there was a greater initial decline in group III animals, there was a negligible recovery from 3 days (35.9±1.5%) to 5 weeks (39.0±1.8% *P*=ns). The ejection fraction of
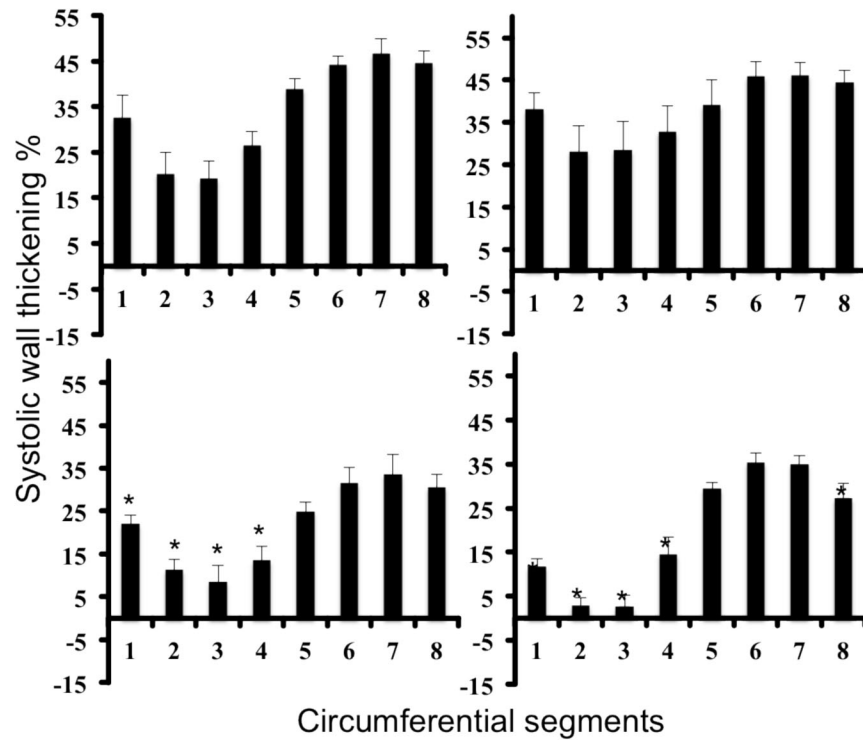

Figure 3. Percent systolic wall thickening of the LV wall in Group II (top) and Group III animals (bottom) at 3 days (left) and 5 weeks (right). The extent of segmental dysfunction is significantly greater after delivery of microemboli in schemically injured myocardium compared with solely 45 min occlusion, suggesting a delayed in the healing process due to microemboli and/or the difference in infarct size.

control animals remained steady throughout the course of the study (50±1% and 51±1% *P*=ns, respectively). The end systolic volume at 3 days (1.3±0.08ml/kg body weight) was significantly greater than 5 weeks (0.9±0.06 *P*<0.05) in group II animals suggesting partial recovery of function. There was no difference in group III animals from 3 days (1.6±0.1ml/kg body weight) to 5 weeks (1.3±0.1 *P*=ns). The end diastolic volume was significantly greater at 3 days (2.3±0.07ml/kg body weight) than at 5 weeks (1.8±0.06 *P*<0.05) in group II animals. Similar to end systolic volume, end diastolic volume showed no difference in group III animals from 3 days (2.4±0.1ml/kg body weight) to 5 weeks (2.2±0.1 *P*=ns). In group I the end systolic and diastolic

volumes at 3 days (2.1±0.1ml/kg body weight and 1.0±0.05ml/kg, respectively) were significantly greater than 5 weeks (1.5±0.09 and 0.7±0.07ml/kg, respectively).

First pass perfusion MRI demonstrated the difference in regional perfusion between the groups (II vs III). Group III demonstrated regional perfusion deficits at 3 days (8/8) and 5 weeks (8/8) compared with group II (5/8 and 3/8 respectively) (Figure 4). These changes were reflected by max upslope, time to max signal intensity and max signal intensity (Tables 1 and 2).

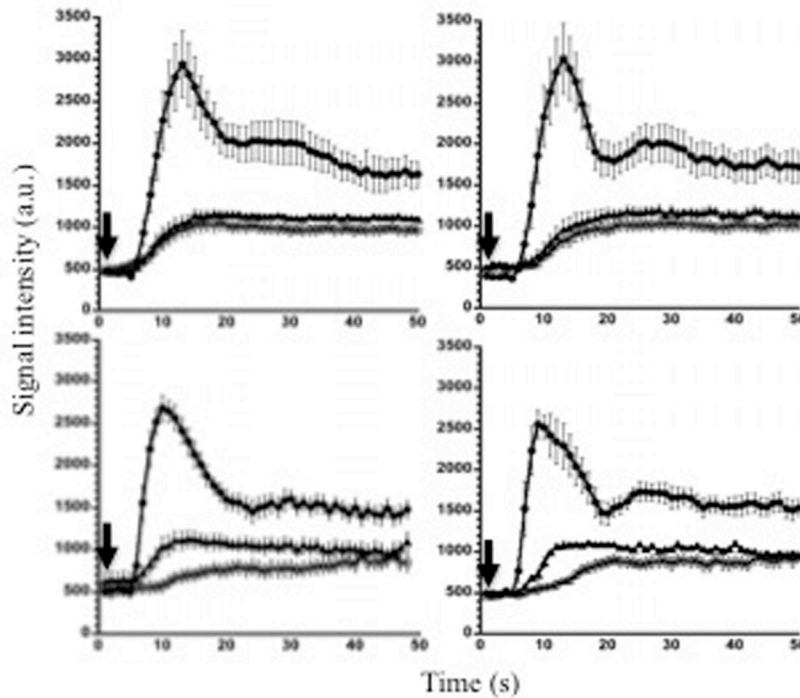**Figure 4.** First pass perfusion plots of Group II (top) and Group III animals (bottom) at 3 days (left) and 5 weeks (right) in 3 regions of interest, namely, LV chamber (solid circles), remote myocardium (solid triangles) and LAD territory (open squares). The arrow indicates the time of injection of Gd-DTPA. Unlike 45 min ischemic myocardium, microembolized ischemic myocardium showed persistent decline in myocardial perfusion.

Table 1: MR perfusion indices of animals subjected to 45 min LAD occlusion/reperfusion (group II) with microembolization (Group III) at 3 days.

	Group II	**Group III**
LV chamber blood		
Max signal intensity	$2.94 \times 10^3 \pm 4.0 \times 10^2$	$2.68 \times 10^3 \pm 1.50 \times 10^2$
Time to peak (s)	6.5 ± 0.8	7.7 ± 1.7
Max upslope	$7.33 \times 10^2 \pm 8.12 \times 10$	$7.71 \times 10^2 \pm 7.04 \times 10$
Remote myocardium		
Max signal intensity	$1.16 \times 10^3 \pm 5.36 \times 10$	$1.13 \times 10^3 \pm 9.54 \times 10$
Time to peak (s)	$1.09 \times 10 \pm 1.4$	$1.12 \times 10 \pm 1.2$
Max upslope	$1.76 \times 10^2 \pm 2.59 \times 10$	$1.70 \times 10^2 \pm 2.19 \times 10$
Infarct		
Max signal intensity	$1.05 \times 10^3 \pm 8.61 \times 10$	$7.93 \times 10^2 \pm 8.65 \times 10$*
Time to peak (s)	$1.20 \times 10 \pm 1.7$	$1.76 \times 10 \pm 1.2$*
Max upslope	$1.82 \times 10^2 \pm 2.84 \times 10$	$1.29 \times 10^2 \pm 2.12 \times 10$*

*P<0.05 compared with 45 min ischemia; group II

Table 2: MR perfusion indices of animals subjected to 45 min LAD occlusion/reperfusion (group II) with microembolization (Group III) at 5 weeks.

	Group II	**Group III**
LV chamber blood		
Max signal intensity	$3.05 \times 10^3 \pm 4.27 \times 10^2$	$2.55 \times 10^3 \pm 1.78 \times 10^2$
Time to peak (s)	6.9 ± 0.7	7.9 ± 1.0
Max upslope	$7.68 \times 10^2 \pm 1.50 \times 10^2$	$7.41 \times 10^2 \pm 1.34 \times 10^2$
Remote myocardium		
Max signal intensity	$1.09 \times 10^3 \pm 9.75 \times 10$	$1.08 \times 10^3 \pm 4.76 \times 10$
Time to peak (s)	$1.24 \times 10 \pm 1.6$	$1.20 \times 10 \pm 1.6$
Max upslope	$1.89 \times 10^2 \pm 2.97 \times 10$	$1.69 \times 10^2 \pm 2.48 \times 10$
Infarct		
Max signal intensity	$1.02 \times 10^3 \pm 6.70 \times 10$	$9.01 \times 10^2 \pm 5.73 \times 10$*
Time to peak (s)	$1.24 \times 10 \pm 1.4$	$1.85 \times 10 \pm 1.9$*
Max upslope	$1.63 \times 10^2 \pm 3.53 \times 10$	$1.18 \times 10^2 \pm 18.5 \times 10$*

*P<0.05 compared with 45 min ischemia; group II

DE-MRI of group II animals showed subendocardial homogeneous infarct at 3 days (3.3±2.2g) and was significantly smaller at 5 weeks (1.3±0.9g). In addition to homogeneous MI,
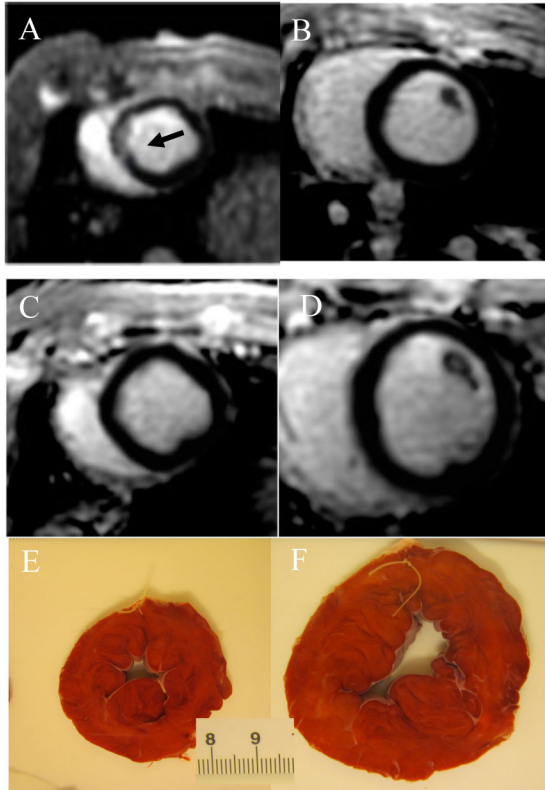

Figure 5. Multi-slice MR images show a representative group II animal at 3 days (A,B) and 5 weeks (C,D) on DE-MRI and TTC histochemical staining (E,F). Subendocardial infarct (black arrow) is evident at 3 days that was resorbed at 5 weeks on DE-MRI. Infarct resorption is more evident in this group compared with double insult animals. TTC confirmed DE-MRI findings at 5 weeks.

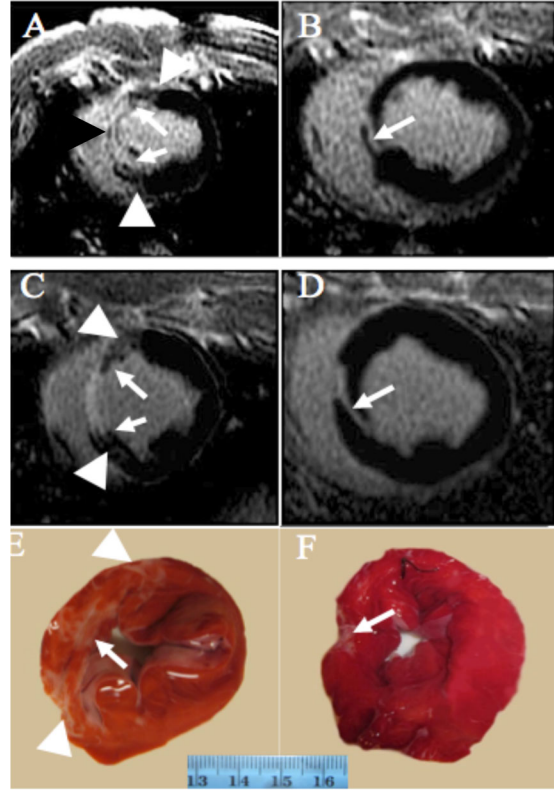**Figure 6.** Multi-slice MR images show a representative group III animal at 3 days (A,B) and 5 weeks (C,D) on DE-MRI and TTC (E,F). Hyperenhanced infarct core and patchy microinfarct (white arrowheads) at peri infarcted region are evident at 3 days and persisted to 5 weeks. Reperfusion MVO is visible as hypoenhanced region in the core of the infarct at 3 days (black arrowhead). TTC confirms DE-MRI findings at 5 weeks.

patchy microinfarct at the border zone was also visible in group III on DE-MRI. TTC staining

confirmed the presence of the infarct in group II and the combination of homogeneous and
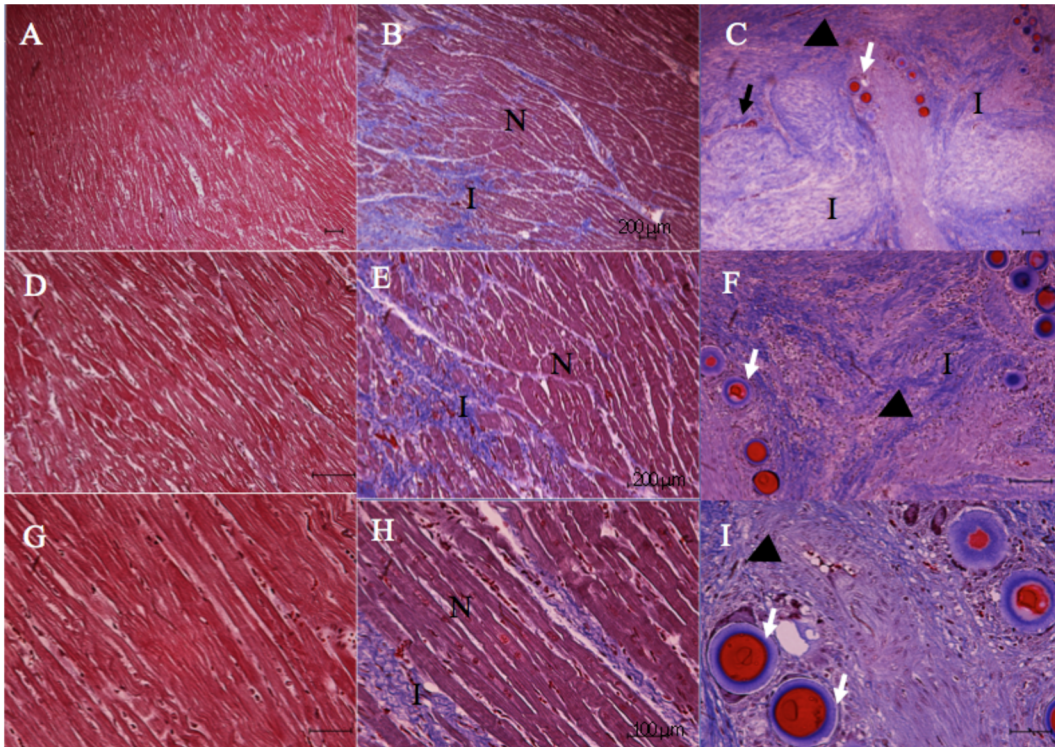

Figure 7. Massons Trichrome staining at 5 weeks for control group I (A,D,G) post intervention for group II (B,E,H) and group III (C,F,I) at low (40X, top row) medium (100X, middle row) and high (200X, bottom row) magnifications, revealed no infarct in normal control animals, the infarct (I) surrounded by normal myocardium (N) in group II and microemboli (black arrows) mechanically obstructing vessels inhibiting infarct healing as documented by the presence of inflammatory cells and extravascular erythrocytes (black arrowheads) in group III animals, as a result persistent hemorrhage (white arrows) was visible on microscopy at 5 weeks after intervention.

patchy microinfarct microembolized ischemic myocardium. At 3 days on DE-MRI, infarct

extent was 9.8±0.6 and was significantly smaller at 5 weeks (7.7±0.5g, *P*<0.05) in group III.

Substantial reduction (60%) in infarct extent was documented in group II, but was significantly

less (22%, *P*<0.05) in group III (Figures 5 and 6). Histochemical TTC at 5 weeks confirmed the

infarct extent on DE-MRI (1.6±1.0g in group II and 9.2±1.6g in group III). Infarct extent was

greater on microscopy in group II (2.8±0.4g) and III (10.5±1.5) than DE-MRI, TTC. The LV

mass was 110±2g (*P*=0.02 compared with groups I and II) in group III, 99±4g in group II and 93±4g in group I. Traces of inflammatory cells/erythrocytes were visible in group III at 5 weeks (Figure 7) suggesting a delay in infarct healing. This delay may extenuate hypertrophy in remote myocardium. At the cellular level collagen, macrophages and remodeled thick-walled vessels were found in microembolized ischemic myocardium at 5 weeks after embolization in group III. Microscopically, histologic sections revealed microemboli mechanically obstructing the vessels (Figure 7).

Discussion

The major findings of this current study are: 1) 45 min ischemia produced homogeneous infarct without visible MVO on DE-MRI at 3 days; 2) The combination of ischemia and microemboli caused homogeneous infarct, patchy microinfarct and MVO at 3 days; 3) Cine MRI revealed decline in LV function compared with controls; 4) At 5 weeks perfusion deficits were evident in animals subjected to ischemia with microembolization and 5) DE-MRI underestimates the extent of scar tissue in group II and in group III, suggesting the limited sensitively of this imaging technique.

LV structure and function

Evidence of edema at 3 days was seen on end diastolic wall thickness within the LAD territory compared with remote myocardium of animals subjected to 45 min occlusion with microemboli followed by reperfusion, whereas animals who underwent solely 45 min occlusion followed by reperfusion showed no significant difference in end diastolic wall thickness, due to less severe injury. At 5 weeks there was significant wall thinning at the LAD territory and compensatory hypertrophy in the remote myocardium in group III animals, where in group II there was no change in end diastolic wall thickness. Wall thinning in group III can be attributed to 1) the slippage of myocyte bundles (47) and 2) infarct resorption during the healing process (16). A recent study showed that the healing and wall thinning can be affected by the presence of MVO (12) and/or absent residual viability (48). This concept has been perpetuated, despite a paucity of experimental data concerning the effects of myocardial ischemia without infarct on diastolic wall thickness (49).

Ongoing LV remodeling is a major determinant of poor prognosis (11). This study reported that reverse remodeling occurred following coronary revascularization in group II

16

animals with substantial myocardial viability and supports previous studies (50-52). In contrast, group III animals showed minor increase but not significant in ejection fraction and negligible changes in LV volumes. Ma et al found a progressive increase in systolic end diastolic volumes 1 week after delivery of microemboli in rats (53). In a longer term study (7-8 weeks), our group found that microemboli produced a permanent decrease in LV ejection fraction (3). In both group I and II animals it was found that end systolic and end diastolic volumes decreased from 3 days to 5 weeks when accounting for the natural enlargement of the heart due to the growth of the animals. We found that the delay in infarct resorption is the primary cause of compensatory hypertrophy that may also occur in the setting of ischemia after PCI (12). This hypothesis requires further investigation.

Microemboli and microinfarct

Visualization of microembolization in clinical routine is limited by the spatial resolution of the current conventional imaging methods. DE-MRI and DE-multidetector computed tomography were inconsistent in demonstrating the effects of small volumes ($<16mm^3$) of 40-120μm microemboli (3, 4, 14, 15, 39) or microinfarct of <5% of the slice (54). On the other hand, cine and first pass perfusion sequences were able to demonstrate the decline in LV function and perfusion after delivery of $16mm^3$ microemboli (15). In the current study, LV dysfunction shown on cine MRI was not consistently associated with a visible infarct in group II at 5 weeks (3/8). Ischemic myocardium with microemboli resulted in deleterious effects on LV function, which were comparable with 90 min LAD occlusion followed by reperfusion (16) with similar resorption percentage in the 45 min LAD occlusion, microembolization followed by reperfusion animals (22% and 24%, respectively). The resorption in group II was significantly greater than in group III. This difference can be attributed to 2 factors: First, the resorption

17

(healing) is faster in small compared with large infarct (55). Secondly, microvascular obstruction inhibits/delays infarct healing and enhances compensatory hypertrophy (12). The later finding has also been observed on MDCT, histochemistry and histologically (56).

Histological examination of group II animals showed small homogeneous infarct that tended to reside nearer to the subendocardial surface and without wall thinning. It is likely that local myocytes in the LAD territory were hypertrophied to compensate for the scar tissue, which was not the case in group III. This study has some limitations, where MRI and histology were performed in a limited number of animals. Longer follow up is needed to monitor the degree of remodeling and infarct extent. Nevertheless, despite these limitations, we believe our study provides new insights into the pathophysiology of microembolized infarct and more broadly on the process of infarct healing. In concordance with the Surgical Treatment in Ischemic Cardiomyopathy sub-study (57), our findings highlight that the pathophysiology of microembolized ischemic myocardium is still incompletely understood and that there is much to improve regarding the assessment of viability on MRI.

Conclusions

Cine, first pass perfusion and viability MRI proved capable of detecting acute and chronic structural and functional changes in microembolized ischemic. Coronary microembolization of ischemic myocardium exacerbates the development of compensatory hypertrophy in remote myocardium. Furthermore, the imaging sequences, histochemical staining and microscopy confirmed ischemia superimposed with microemboli. While, DE-MRI has the potential to monitor infarct resorption, the limited spatial resolution for detecting microinfarcts must be accounted for when DE-MRI is used to test the efficacy of cardioprotective therapies and distal protective devices in improving LV function and healing.

References:

1. Carlsson M, Jablonowski R, Martin AJ, Ursell PC, Saeed M. Coronary microembolization causes long-term detrimental effects on regional left ventricular function. Scand Cardiovasc J 2011.
2. Carlsson M, Martin AJ, Ursell PC, Saloner D, Saeed M. Magnetic resonance imaging quantification of left ventricular dysfunction following coronary microembolization. Magn Reson Med 2009; 61:595-602.
3. Carlsson M, Saloner D, Martin AJ, Ursell PC, Saeed M. Heterogeneous microinfarcts caused by coronary microemboli: evaluation with multidetector CT and MR imaging in a swine model. Radiology 2010; 254:718-728.
4. Carlsson M, Wilson M, Martin AJ, Saeed M. Myocardial microinfarction after coronary microembolization in swine: MR imaging characterization. Radiology 2009; 250:703-713.
5. Dicks DL, Carlsson M, Heiberg E, et al. Persistent decline in longitudinal and radial strain after coronary microembolization detected on velocity encoded phase contrast magnetic resonance imaging. J Magn Reson Imag 2009; 30:69-76.
6. Saeed M. An overview of the consequences of distal coronary microembolization on left ventricular function, perfusion and viability. Int J Clin Med 2011; 2:40-50.
7. Anderson JL, Adams CD, Antman EM, et al. ACC/AHA 2007 guidelines for the management of patients with unstable angina/non-ST-Elevation myocardial infarction: a report of the American College of Cardiology/American Heart Association Task Force on Practice Guidelines (Writing Committee to Revise the 2002 Guidelines for the Management of Patients With Unstable Angina/Non-ST-Elevation Myocardial Infarction) developed in collaboration with the American College of Emergency Physicians, the Society for Cardiovascular Angiography and Interventions, and the Society of Thoracic Surgeons endorsed by the American Association of Cardiovascular and Pulmonary Rehabilitation and the Society for Academic Emergency Medicine. J Am Coll Cardiol 2007; 50:e1-e157.
8. Pislaru SV, Barrios L, Stassen T, Jun L, Pislaru C, Van de Werf F. Infarct size, myocardial hemorrhage, and recovery of function after mechanical versus pharmacological reperfusion: effects of lytic state and occlusion time. Circulation 1997; 96:659-666.
9. Ganame J, Messalli G, Dymarkowski S, et al. Impact of myocardial haemorrhage on left ventricular function and remodelling in patients with reperfused acute myocardial infarction. Eur Heart J 2009; 30:1440-1449.
10. van der Laan AM, Nahrendorf M, Piek JJ. Republished: healing and adverse remodelling after acute myocardial infarction: role of the cellular immune response. Postgrad Med J 2013; 89:52-58.
11. Wu KC. CMR of microvascular obstruction and hemorrhage in myocardial infarction. Journal of cardiovascular magnetic resonance : official journal of the Society for Cardiovasc Magn Reson 2012; 14:68.
12. Bajwa HZ, Do L, Suhail M, Hetts SW, Wilson MW, Saeed M. MRI demonstrates a decrease in myocardial infarct healing and increase in compensatory ventricular hypertrophy following mechanical microvascular obstruction. J Magn Reson Imag 2014.

13. Saeed M. MR Assessment of myocardial viability and microvascular integrity in ischemic heart disease. Cur Med Imaging Rev 2006; 2:299-314.

14. Saeed M, Hetts SW, Do L, Wilson MW. MRI study on volume effects of coronary emboli on myocardial function, perfusion and viability. Int J Cardiol 2013; 165:93-99.

15. Saeed M, Hetts SW, Ursell PC, Do L, Kolli KP, Wilson MW. Evaluation of the acute effects of distal coronary microembolization using multidetector computed tomography and magnetic resonance imaging. Magn Reson Med 2012; 67:1747-1757.

16. Saeed M, Lee RJ, Weber O, et al. Scarred myocardium imposes additional burden on remote viable myocardium despite a reduction in the extent of area with late contrast MR enhancement. Eur Radiol 2006; 16:827-836.

17. Saeed M, Martin A, Ursell P, et al. MR assessment of myocardial perfusion, viability, and function after intramyocardial transfer of VM202, a new plasmid human hepatocyte growth factor in ischemic swine myocardium. Radiology 2008; 249:107-118.

18. Heusch G, Skyschally A, Schulz R. The in-situ pig heart with regional ischemia/reperfusion - ready for translation. J Mol Cell Cardiol 2011; 50:951-963.

19 Saeed M, Saloner D, Martin A, et al. Adeno-associated viral vector-encoding vascular endothelial growth factor gene: effect on cardiovascular MR perfusion and infarct resorption measurements in swine. Radiology 2007; 243:451-460.

20. Saber RS, Edwards WD, Bailey KR, McGovern TW, Schwartz RS, Holmes DR, Jr. Coronary embolization after balloon angioplasty or thrombolytic therapy: an autopsy study of 32 cases. J Am Coll Cardiol 1993; 22:1283-1288.

21. Schwartz RS, Burke A, Farb A, et al. Microemboli and microvascular obstruction in acute coronary thrombosis and sudden coronary death: relation to epicardial plaque histopathology. J Am Coll Cardiol 2009; 54:2167-2173.

22. Gick M, Jander N, Bestehorn HP, et al. Randomized evaluation of the effects of filter-based distal protection on myocardial perfusion and infarct size after primary percutaneous catheter intervention in myocardial infarction with and without ST-segment elevation. Circulation 2005; 112:1462-1469.

23. Guetta V, Mosseri M, Shechter M, et al. Safety and efficacy of the FilterWire EZ in acute ST-segment elevation myocardial infarction. Am J Cardiol 2007; 99:911-915.

24. Cura FA, Escudero AG, Berrocal D, et al. Protection of Distal Embolization in High-Risk Patients with Acute ST-Segment Elevation Myocardial Infarction (PREMIAR). Am J Cardiol 2007; 99:357-363.

25. Sangiorgi G, Colombo A. Embolic protection devices. Heart 2003; 89:990-992.

26. Chen CI, Iguchi Y, Garami Z, et al. Analysis of emboli during carotid stenting with distal protection device. Cerebrovasc Dis 2006; 21:223-228.

27. Flach HZ, Ouhlous M, Hendriks JM, et al. Cerebral ischemia after carotid intervention. J Endovasc Ther 2004; 11:251-257.

28. Choi JW, Gibson CM, Murphy SA, Davidson CJ, Kim RJ, Ricciardi MJ. Myonecrosis following stent placement: association between impaired TIMI myocardial perfusion grade and MRI visualization of microinfarction. Catheter Cardiovasc Interv 2004; 61:472-476.

29. Selvanayagam JB, Cheng AS, Jerosch-Herold M, et al. Effect of distal embolization on myocardial perfusion reserve after percutaneous coronary intervention: a quantitative magnetic resonance perfusion study. Circulation 2007; 116:1458-1464.

30. Ricciardi MJ, Wu E, Davidson CJ, et al. Visualization of discrete microinfarction after percutaneous coronary intervention associated with mild creatine kinase-MB elevation. Circulation 2001; 103:2780-2783.

31. Porto I, Biasucci LM, De Maria GL, et al. Intracoronary microparticles and microvascular obstruction in patients with ST elevation myocardial infarction undergoing primary percutaneous intervention. Eur Heart J 2012; 33:2928-2938.

32. Porto I, Selvanayagam JB, Van Gaal WJ, et al. Plaque volume and occurrence and location of periprocedural myocardial necrosis after percutaneous coronary intervention: insights from delayed-enhancement magnetic resonance imaging, thrombolysis in myocardial infarction myocardial perfusion grade analysis, and intravascular ultrasound. Circulation 2006; 114:662-669.

33. Limbruno U, De Carlo M, Pistolesi S, et al. Distal embolization during primary angioplasty: histopathologic features and predictability. Am Heart J 2005; 150:102-108.

34. Indik JH, Allen D, Gura M, Dameff C, Hilwig RW, Kern KB. Utility of the ventricular fibrillation waveform to predict a return of spontaneous circulation and distinguish acute from post myocardial infarction or normal Swine in ventricular fibrillation cardiac arrest. Circulation. Arrhyth and Electrophysiol 2011; 4:337-343.

35. Saeed M, Hetts SW, Do L, Wilson MW. Coronary microemboli effects in preexisting acute infarcts in a swine model: cardiac MR imaging indices, injury biomarkers, and histopathologic assessment. Radiology 2013; 268:98-108.

36. Burstein D, Taratuta E, Manning WJ. Factors in myocardial "perfusion" imaging with ultrafast MRI and Gd-DTPA administration. Magnetic resonance in medicine : official journal of the Society of Magn Reson Med 1991; 20:299-305.

37. Heiberg E, Ugander M, Engblom H, et al. Automated quantification of myocardial infarction from MR images by accounting for partial volume effects: animal, phantom, and human study. Radiology 2008; 246:581-588.

38. O'Regan DP, Ahmed R, Neuwirth C, et al. Cardiac MRI of myocardial salvage at the peri-infarct border zones after primary coronary intervention. American journal of physiology. Heart and Circ Physiol 2009; 297:H340-346.

39. Nassenstein K, Breuckmann F, Bucher C, et al. How much myocardial damage is necessary to enable detection of focal late gadolinium enhancement at cardiac MR imaging? Radiology 2008; 249:829-835.

40. Saeed M. Value of blood pool MR contrast agents in imaging of the heart and blood vessels. Drugs Today (Barc) 1999; 35:879-892.

41. Saeed M. New concepts in characterization of ischemically injured myocardium by MRI. Exp Biol Med (Maywood) 2001; 226:367-376.

42. Saeed M, Bremerich J, Wendland MF, Wyttenbach R, Weinmann HJ, Higgins CB. Reperfused myocardial infarction as seen with use of necrosis-specific versus standard extracellular MR contrast media in rats. Radiology 1999; 213:247-257.

43. Saeed M, Higgins CB, Geschwind JF, Wendland MF. T1-relaxation kinetics of extracellular, intracellular and intravascular MR contrast agents in normal and acutely reperfused infarcted myocardium using echo-planar MR imaging. Eur Radiol 2000; 10:310-318.

44. Heusch G, Schulz R, Haude M, Erbel R. Coronary microembolization. J Mol Cell Cardiol 2004; 37:23-31.
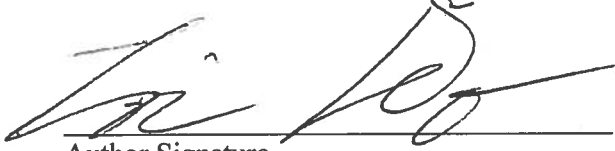
45. Saeed M, Martin A, Jacquier A, et al. Permanent coronary artery occlusion: cardiovascular MR imaging is platform for percutaneous transendocardial delivery and assessment of gene therapy in canine model. Radiology 2008; 249:560-571.

46. Lautamaki R, Schuleri KH, Sasano T, et al. Integration of infarct size, tissue perfusion, and metabolism by hybrid cardiac positron emission tomography/computed tomography: evaluation in a porcine model of myocardial infarction. Circulation. Cardiovascular imaging 2009; 2:299-305.

47. Weisman HF, Bush DE, Mannisi JA, Weisfeldt ML, Healy B. Cellular mechanisms of myocardial infarct expansion. Circulation 1988; 78:186-201.

48. Weisman HF, Healy B. Myocardial infarct expansion, infarct extension, and reinfarction: pathophysiologic concepts. Progr Cardiovasc Dis 1987; 30:73-110.

49. Koyama Y, Matsuoka H, Mochizuki T, et al. Assessment of reperfused acute myocardial infarction with two-phase contrast-enhanced helical CT: prediction of left ventricular function and wall thickness. Radiology 2005; 235:804-811.

50. Carluccio E, Biagioli P, Alunni G, et al. Patients with hibernating myocardium show altered left ventricular volumes and shape, which revert after revascularization: evidence that dyssynergy might directly induce cardiac remodeling. Journal of the Am Col Cardiol 2006; 47:969-977.

51. Rizzello V, Poldermans D, Boersma E, et al. Opposite patterns of left ventricular remodeling after coronary revascularization in patients with ischemic cardiomyopathy: role of myocardial viability. Circulation 2004; 110:2383-2388.

52. Pasquet A, Lauer MS, Williams MJ, Secknus MA, Lytle B, Marwick TH. Prediction of global left ventricular function after bypass surgery in patients with severe left ventricular dysfunction. Impact of pre-operative myocardial function, perfusion, and metabolism. Eur Heart J 2000; 21:125-136.

53. Ma JY, Qian JY, Jin H, et al. Acute hyperenhancement on delayed contrast-enhanced magnetic resonance imaging is the characteristic sign after coronary microembolization. Chin Med J 2009; 122:687-691.

54. Heusch G, Kleinbongard P, Bose D, et al. Coronary microembolization: from bedside to bench and back to bedside. Circulation 2009; 120:1822-1836.

55. Lund GK, Stork A, Muellerleile K, et al. Prediction of left ventricular remodeling and analysis of infarct resorption in patients with reperfused myocardial infarcts by using contrast-enhanced MR imaging. Radiology 2007; 245:95-102.

56. Saeed M, Hetts SW, Do L, Sullivan S, Wilson MW. MDCT has the potential to predict percutaneous coronary intervention outcome in swine model: microscopic validation. Acta Radiol 2012; 53:987-994.

57. Bonow RO, Maurer G, Lee KL, et al. Myocardial viability and survival in ischemic left ventricular dysfunction. New Engl J Med 2011; 364:1617-1625.
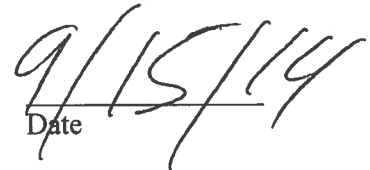
Publishing Agreement

It is the policy of the University to encourage the distribution of all theses, dissertations, and manuscripts. Copies of all UCSF theses, dissertations, and manuscripts will be routed to the library via the Graduate Division. The library will make all theses, dissertations, and manuscripts accessible to the public and will preserve these to the best of their abilities, in perpetuity.

Please sign the following statement:

I hereby grant permission to the Graduate Division of the University of California, San Francisco to release copies of my thesis, dissertation, or manuscript to the Campus Library to provide access and preservation, in whole or in part, in perpetuity.

_____   9/15/14
Author Signature   Date

23